

Communication

An Efficient Zr-ZSM-5-st Solid Acid Catalyst for the Polyol Esterification Reaction

Huaigang Su^{1,2}, Ze Zong³, Wenjing Lou^{1,4} , Qin Zhao^{1,4}, Xiaobo Wang^{1,4}, Xiang Feng³, Yanxing Qi^{1,*} and Zhaoning Song^{3,*}

¹ State Key Laboratory of Solid Lubrication, National Engineering Research Center for Fine Petrochemical Intermediates, Lanzhou Institute of Chemical Physics, CAS, Lanzhou 730000, China

² University of Chinese Academy of Sciences, Beijing 100049, China

³ State Key Laboratory of Heavy Oil Processing, China University of Petroleum, Qingdao 266580, China

⁴ Qingdao Center of Resource Chemistry and New Materials, Qingdao 266100, China

* Correspondence: qiyx@licp.cas.cn (Y.Q.); songzhaoning@outlook.com (Z.S.)

Abstract: In this study, Zr active species were implanted into a ZSM-5 zeolite framework to form a solid acid catalyst through steam treatment and the liquid-solid isomorphous substitution process. The as-synthesized Zr-ZSM-5-st catalyst ensured excellent esterification of trimethylolpropane and fatty acids (FAs) to achieve a polyol ester production yield of 94.41%. Combined with N₂ physisorption, X-ray diffraction, Fourier transform infrared spectroscopy, ultraviolet-visible spectroscopy, transmission electron microscopy mapping, X-ray photoelectron spectroscopy, NH₃ temperature-programmed desorption, and inductively coupled mass plasma spectroscopy were conducted. The results revealed that the excellent performance of Zr-ZSM-5-st catalyst could be attributed to the enhanced acidity and the developed surface area and pore structure.

Keywords: Zr-containing solid acid catalyst; ZSM-5 zeolite; polyol ester; esterification; lubricating ester oils



Citation: Su, H.; Zong, Z.; Lou, W.; Zhao, Q.; Wang, X.; Feng, X.; Qi, Y.; Song, Z. An Efficient Zr-ZSM-5-st Solid Acid Catalyst for the Polyol Esterification Reaction. *Catalysts* **2022**, *12*, 901. <https://doi.org/10.3390/catal12080901>

Academic Editors: Valeria La Parola and Leonarda Francesca Liotta

Received: 21 July 2022

Accepted: 15 August 2022

Published: 16 August 2022

Publisher's Note: MDPI stays neutral with regard to jurisdictional claims in published maps and institutional affiliations.



Copyright: © 2022 by the authors. Licensee MDPI, Basel, Switzerland. This article is an open access article distributed under the terms and conditions of the Creative Commons Attribution (CC BY) license (<https://creativecommons.org/licenses/by/4.0/>).

1. Introduction

Synthetic lubricating oils (SLOs) exhibit considerable potential for use in numerous applications because of their stable and unique molecular structures, which results in excellent high/low temperature resistance, viscosity–temperature performance, flame resistance, and oxidation stability [1,2]. Polyol esters (POEs) are a type of high value and efficient SLOs because of their high thermostability, viscosity, and biodegradability. SLOs are typically prepared by esterifying carboxylic acids with the multi-hydroxyl groups (polyol)-containing alcohol by using acidic catalysts. Efficient industrial esterification catalysts such as sulfuric acid and hydrofluoric acid are acidic catalysts with high homogeneity. However, homogeneous acid catalysts cause severe environmental problems and their technical separation remains a concern. For solving the problems caused by homogeneous acid catalysts, heterogeneous acidic catalysts such as solid acid catalysts have attracted considerable research attention.

Among the solid acid catalysts, SO₄²⁻/ZrO₂ catalysts exhibit excellent performance in the esterification reaction because of their excellent acid strength, renewability, noncorrosiveness, and nonpolluting characteristics [3,4]. However, their low surface areas and irregular pore structure result in poor mass transfer and catalytic selectivity, which limits their application. Though conversion close to 100% and very high selectivity to triesters can be obtained in the presence of a silica zirconia amorphous catalyst by F. Zaccheria [5], there is still a strong demand for novelty catalyst. By contrast, ZSM-5 zeolite with large surface area, excellent shape-selectivity, excellent hydrothermal stability, and tunable microstructure properties (crystal size, pore structure, acidity) have been widely used as a catalyst [6–10]. However, compared with the conventional esterification catalysts, the

acidity of the ZSM-5 zeolite is too weak to facilitate adequate esterification [11]. Therefore, the development of a novel efficient solid acid zeolite catalyst through modification of the ZSM-5 zeolite is critical. The incorporation of transition metal heteroatoms such as Fe, Ti, Cu, and Zr into the zeolite framework has been studied extensively [12,13]. Materials that contain Zr have attracted considerable interests because zirconium (Zr) exhibits advantages such as enhancing the acidity of the synthesized materials. Zr^{4+} with a high oxidation state exhibits considerable potential to accept electrons. Therefore, its compounds exhibit strong Lewis acid acidity, which is conducive to catalyzing a series of esterification reactions [14–16]. Therefore, the development of environment-friendly esterification catalysts by combining the strong acidity of Zr species with the structural advantages of ZSM-5 zeolite is crucial.

In this study, a novel strategy was developed to implant Zr species into the MFI framework through steaming treatment combined with the liquid–solid identical crystal substitution method. The as-synthesized Zr-ZSM-5 catalyst exhibits excellent catalytic performance in the esterification reaction. Such structure–performance relation of Zr-ZSM-5-st catalyst has been comprehensively studied through several characterizations, such as Fourier transform infrared spectroscopy (FT-IRS), ultraviolet-visible spectroscopy (UV-vis), X-ray photoelectron spectroscopy (XPS), NH_3 -TPD, transmission electron microscopy mapping (TEM-mapping), X-ray diffraction (XRD), N_2 physisorption, and inductive coupled plasma optical emission spectrometry (ICP-OES). The implanted framework Zr species elevates strong acid site quantity, whereas the developed surface area and pore structure of Zr-ZSM-5-st improves mass transfer ability, thus enhancing catalytic efficiency. This study contributes to designing and synthesizing Zr-containing solid acid catalysts with high efficiency for esterification reactions. Furthermore, this study investigated the reusability of analyzed composite catalysts.

2. Results and Discussion

2.1. Catalyst Characterization

A series of Zr-ZSM-5-st samples were prepared through steam treatment and liquid–solid isomorphous substitution method introducing Zr^{4+} species. According to Figure 1a, a Zr(40)-ZSM-5-st(500) sample maintained typical MFI topological diffraction peaks after steam treatment and Zr implantation. Furthermore, no diffraction peak of Zr species was observed, which indicated that Zr species are highly dispersed in Zr(40)-ZSM-5-st(500) without agglomeration. With the increase in the steam treatment temperature from 400 to 700 °C, the crystallinity of Zr-ZSM-5-st samples decreased (Figure S1a) because steam treatment could remove Al species from the zeolite framework, which resulted in the zeolite framework being destroyed [17]. Moreover, with the decrease in the Si/Zr mole ratio from 133 to 12 (Figure S1b), a diffraction peak appeared at $2\theta = 11.6^\circ$, which represents the strong agglomeration of Zr species in Zr(12)-ZSM-5-st(500). Therefore, XRD results revealed that the Zr(40)-ZSM-5-st(500) sample can maintain excellent crystallinity, and the Zr species were evenly dispersed in the zeolite framework.

Figure 1b displays the FT-IR spectra of Zr(40)-ZSM-5-st(500) and ZSM-5 samples. The Zr(40)-ZSM-5-st(500) sample exhibited a novel band at 962 cm^{-1} compared with the parent ZSM-5 zeolite, which can be ascribed to the antisymmetric stretching vibration of the Si–O–Zr bond within the framework [18]. The aforementioned findings revealed that Zr species are efficiently added to Zr(40)-ZSM-5-st(500). Furthermore, UV-vis spectra were obtained to determine Zr species compositions (Figure 1c). UV-vis results revealed that Zr(40)-ZSM-5-st(500) exhibited a dominant adsorption peak at approximately 207 nm, which is associated with Zr^{4+} tetrahedral species, which revealed that Zr^{4+} species was introduced into the zeolite framework [19]. No adsorption peak of extra-framework ZrO_2 was detected at 230 nm, which indicated no bulk ZrO_2 phase within Zr(40)-ZSM-5-st(500) [19,20]. Moreover, a broad band can be detected at approximately 266 nm in Zr(40)-ZSM-5-st(500). This band can be associated with the separated $(Si-O)_2-Zr=O$ species onto the zeolite framework surface [18,19].

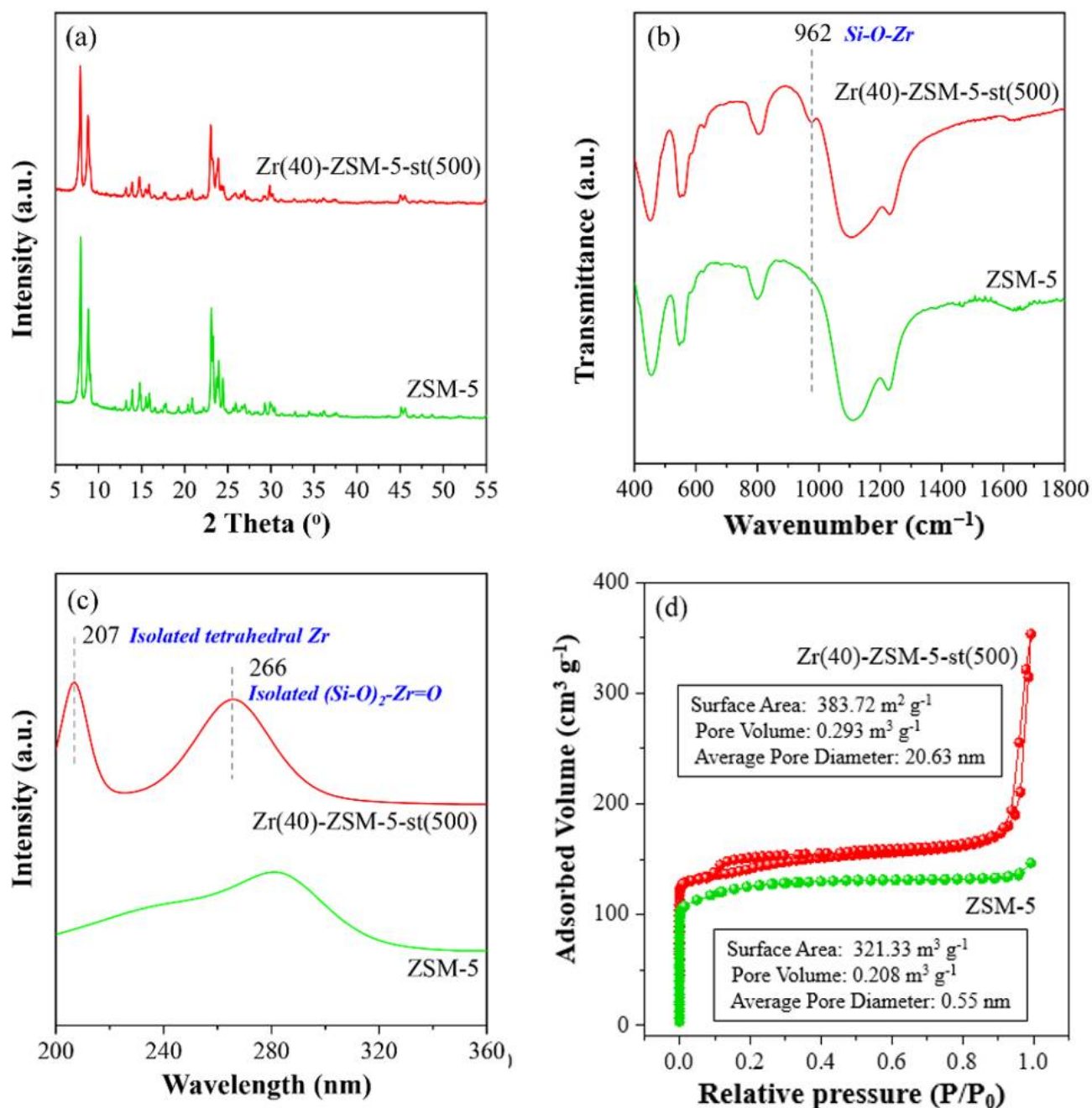


Figure 1. (a) X-ray diffraction (XRD), (b) Fourier transform infrared (FT-IR), (c) ultraviolet-visible spectra as well as (d) N₂ adsorption–desorption isotherms for ZSM-5 with Zr(40)-ZSM-5-st(500) catalysts.

Figure 1d displays the N₂ adsorption–desorption isotherms for Zr(40)-ZSM-5-st(500) and ZSM-5 samples. Figure 1d reveals that the steam treatment process considerably affected the Zr(40)-ZSM-5-st(500) pore structure. Relative to the ZSM-5 product, Zr(40)-ZSM-5-st(500) sample considerably improved the mean pore diameter, pore volume, and the surface area, which was attributed to the destruction of micropores and the formation of secondary intracrystalline and inter-crystalline mesoporous caused by the dealumination of zeolite during steam treatment process [21,22]. Considering the synergistic reaction of catalysis, the developed pore structure was conducive to the mass transfer diffusion of reactants and products. When the steam treatment temperature increased to 700 °C (Table S1), the surface area decreased from 383.72 to 325.21 m²/g, which was attributed to the collapse of the inter-crystalline mesoporous of Zr-ZSM-5-st caused by the high

temperature of steam treatment [23]. Therefore, the Zr(40)-ZSM-5-st(500) sample exhibited the most optimized pore structure when the steam treatment temperature was 500 °C.

The TEM and TEM-mapping images of Zr(40)-ZSM-5-st(500) sample are displayed in Figure 2. Compared with ZSM-5 (Figure S2), the Zr(40)-ZSM-5-st(500) sample exhibited obvious defective structure and excellent crystallinity. Moreover, TEM-mapping images revealed that Zr species were evenly dispersed in the Zr(40)-ZSM-5-st(500) sample because in the process of liquid–solid isomorphous substitution, Zr species easily bonded with the widely distributed defective sites [24].

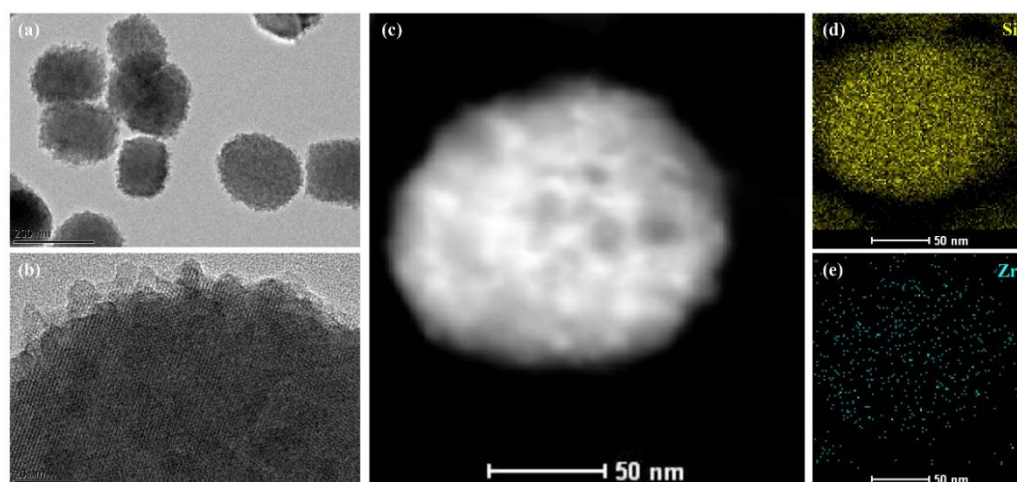


Figure 2. (a,b) TEM and (c–e) TEM-mapping images of Zr(40)-ZSM-5-st(500) catalyst.

The plausible formation mechanism of Zr-ZSM-5-st illustrated in Figure 3 is speculated to proceed as follows: (i) Al element was removed from the ZSM-5 zeolite framework through steam treatment; (ii) Zr species were implanted and bonded to the defective sites formed after dealuminization through liquid–solid isomorphous substitution process.

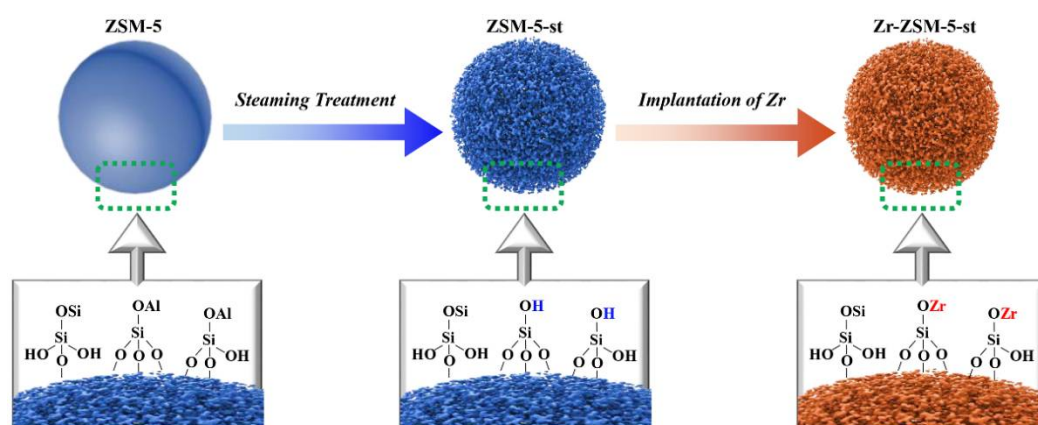


Figure 3. Plausible formation mechanism of the Zr-ZSM-5-st catalyst.

Figure 4a displays the Zr 3d XPS spectra for the Zr(40)-ZSM-5-st(500) sample as well as ZrO_2 . The binding energy values at 184.27 (Zr 3d_{5/2}) together with 186.67 eV (Zr 3d_{3/2}) were observed for Zr(40)-ZSM-5-st(500), which considerably shifted with respect to that of ZrO_2 at 182.21 (Zr 3d_{5/2}) with 184.61 eV (Zr 3d_{3/2}). These shifts in the binding energies of Zr 3d were attributed to the introduced Zr ions to the zeolite framework for forming Si–O–Zr bonds because diverse electronegativity (Si atom > Zr atom) results in increased zirconium positive charges [16,19].

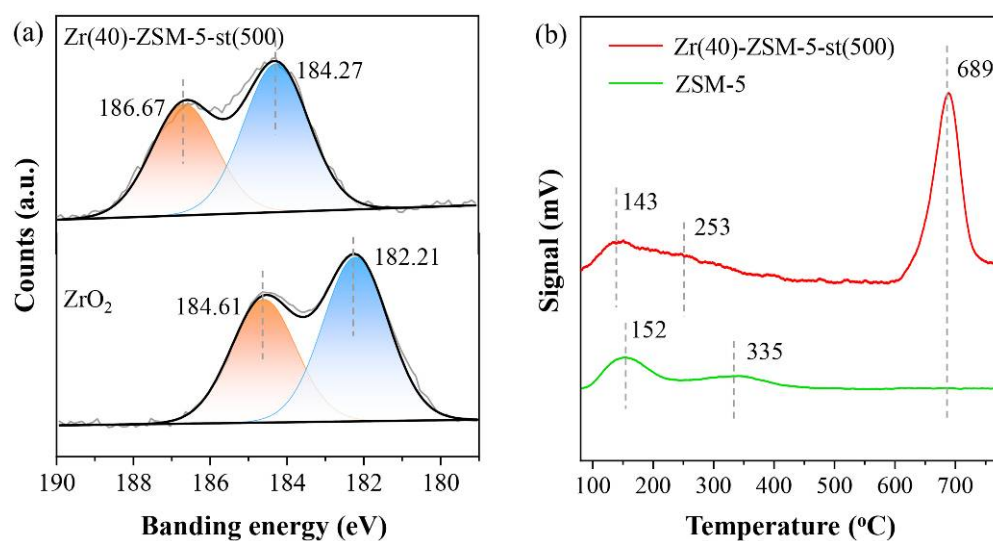


Figure 4. (a) Zr 3d XPS spectra for Zr(40)-ZSM-5-st(500) catalyst as well as ZrO₂. (b) NH₃-TPD spectra for Zr(40)-ZSM-5-st(500) together with ZSM-5 catalysts.

Esterification reaction performance is closely related to the acid properties of the catalyst. NH₃-TPD was adopted in Figure 4b to determine the total acidity of Zr(40)-ZSM-5-st(500) and ZSM-5 samples. Both samples exhibited an NH₃ desorption peak at 140–160 °C, which can be associated with weak acid centers. ZSM-5 exhibited the moderate-strong acid desorption peak at 339 °C, whereas Zr(40)-ZSM-5-st(500) revealed a moderate-strong acid desorption shoulder peak shift to a temperature of 253 °C, which was caused by the dealumination during steam treatment [25]. Furthermore, Zr(40)-ZSM-5-st(500) exhibited a strong acid desorption peak at 689 °C, which was attributed to the superacid site formed by the implanted Zr binding with the zeolite defective sites after steam treatment.

Thus, through steam treatment and liquid–solid isomorphous substitution, Zr⁴⁺ species were introduced into the ZSM-5 zeolite framework. Moreover, for the Zr(40)-ZSM-5-st(500) sample, excellent crystallinity was maintained, mass transfer ability was improved, and Zr⁴⁺ species were evenly dispersed into the zeolite framework. Furthermore, Zr(40)-ZSM-5-st(500) sample exhibited strong acid strength because of the implanted Zr species.

2.2. Catalytic Activity Test

The performance of ZSM-5, Zr-ZSM-5, and diverse Zr-ZSM-5-st catalysts prepared through steam treatment and liquid–solid isomorphous substitution for catalysis were systematically investigated through the esterification of TMP with *n*-caprylic acid (Table 1). The catalytic behavior in the esterification of TMP with *n*-caprylic acid was chosen for the reaction scheme because of the reaction is widely representative. As shown in Table 1, the reaction yield of ZSM-5 was only slightly higher than that of the blank experiment (Table 1, entry 1–2), which indicated that ZSM-5 exhibited weak catalytic activity because its acid strength was insufficient and its microporous structure was not conducive to mass transfer for esterification reaction. Subsequently, the effect of implanted Zr species on the catalytic performance was investigated in detail. For the Zr-ZSM-5 sample without steam treatment, its reaction yield increased from 80.51% to 88.33% primarily because the implanted Zr species exhibited a strong ability to accept electrons, which formed the strong acid centers (Table 1, entry 3). However, Zr-ZSM-5-st catalysts treated with steam exhibited excellent catalytic ability and outperformed Zr-ZSM-5. For proportion of the Si/Zr molar ratio (12, 40, 67, 133) under the same steam treatment (500 °C), the reaction yield of product with Zr(12)-ZSM-5-st(500) catalyst was higher than others (Table 1, entry 10). As the proportion of Zr increases, the residual Zr in the product also increases correspondingly, which is not an ideal result. However, when the proportion decreases to 40, the reaction yield of

product was still higher with 94.41%. This phenomenon shows that the introduction of Zr on ZSM-5 only needs a certain proportion to achieve a good catalytic effect. As for steam temperature from 400 °C to 700 °C, the ideal temperature was 500 °C. This shows that the higher the temperature of steam treatment, the catalytic activity is not better. Among those Zr-ZSM-5-st samples prepared at various steam treatment temperatures and different Si/Zr, the best reaction yield of 94.41% was achieved for Zr(40)-ZSM-5-st(500) (Table 1, entry 5), which was probably associated with strong acidity (Figure S3) as well as superior mass transfer capacity (Table S1). The results of the activity tests show that the steam treatment and introduction of Zr on ZSM-5 has a positive effect on triglycerides conversion and yield of products.

Table 1. Catalytic activities for ZSM-5, Zr-ZSM-5 as well as various Zr-ZSM-5-st catalysts for lubricating ester synthesis reaction.

Catalyst ^a	TAN ^b	Yield ^c (%)	Zr (wt.%) ^d	Al (wt.%) ^e
None	75.0	80.51	0	0
ZSM-5	63.1	82.32	0	1.35
Zr(40 ^f)-ZSM-5	42.7	88.33	4.63	1.34
Zr(40)-ZSM-5-st(400 ^g)	29.7	91.91	4.79	1.07
Zr(40)-ZSM-5-st(500)	20.9	94.41	4.77	0.95
Zr(40)-ZSM-5-st(600)	20.2	94.38	4.81	0.88
Zr(40)-ZSM-5-st(700)	25.9	92.82	4.74	0.82
Zr(133)-ZSM-5-st(500)	55.13	84.72	1.30	0.96
Zr(67)-ZSM-5-st(500)	31.89	91.39	2.44	0.94
Zr(12)-ZSM-5-st(500)	19.9	94.47	10.37	0.94

^a Reaction conditions: 3 mL toluene, 0.045 mol FA, 0.015 mol trimethylolpropane and 0.045 mol *n*-caprylic acid; reaction time and temperature: 5 h and 160 °C, respectively. ^b Total Acid Number: ASTM D 974 was used to test the value, which was subsequently used in determining conversion: conversion (%) = [(1 – reacted acid value/unreacted acid value) × $n_{\text{acid}}/n_{\text{alcohol}}/3$] × 100%. ^c Yield: HR-MS and ¹H NMR were performed to identify products. TMP served as the endogenous control to determine the yield based on ¹H NMR. ^d Zr element level measured through ICP-OES. ^e Al element level measured through ICP-OES. ^f This value represents Si/Zr mole ratio. ^g This value represents steam treatment temperature.

The Zr-ZSM-5-st catalyst exhibits superb catalytic activity, and its mechanism is elaborated as follows. First, implanted framework Zr species elevate strong acid site quantity while improving catalytic activity; second, the developed surface area and pore structure for Zr-ZSM-5-st improved catalytic mass transfer ability.

The stability of the Zr(40)-ZSM-5-st(500) catalyst was tested according to the reusability test, as displayed in Figure 5. Following six cycles of TMP-*n*-caprylic esterification, the obtained catalyst exhibited reduced activity. The yield of TMP ester reflected catalyst stability, and the value was approximately 90%. HR-MS and ¹H NMR were conducted for identifying products, with triphenylmethane used as the endogenous reference to determine the yield based on ¹H NMR. Supplementary materials display details of the procedure.

2.3. Discussion

The catalyst plays an indispensable role in the catalytic process of preparing oil by the reaction of acid and alcohol with high molecular weight and large steric structure. As a common molecular sieve catalyst, ZSM-5 has low acidity and is not suitable for the esterification of TMP with *n*-caprylic acid from the above results. Kiss et al. [26] posited that lower catalytic activity of zeolites is due to the small pores, which limit diffusion of large fatty acid molecules. Heterogeneous catalysts such as ZnO, SnO or ZrO show high activity at T > 160 °C, but form small amounts of soaps that are hardly removed [5]. Interestingly, the structure of ZSM-5 also allows the introduction of alternative T-atoms during synthesis [27]. Sani et al. [28] reported that Zr/ZSM-5 exhibited highest total acidity (0.75 mmol/g), and activity in converting > 95% used frying oil (48 wt.%) over SZr/Ag, SZr/Ti, and SZr/W. Inspired by the above methodologies, Zr²⁺ species was introduced in the positive ion of ZSM-5 by liquid–solid isomorphous substitution method in this paper.

The results showed that the ratio of Zr^{2+} species determines the acidic catalytic power. In addition, Almutairi et. al. [29] considered that steam treatment helps to increase the acid content of Brønsted acid for ZSM catalytic reaction. Thus, steam treatment of Zr(40)-ZSM-5 obviously enhanced the esterification capacity from the results of Table 1.

No matter what the methane sulfonic acid or heterogeneous-like solid acids are used in traditional industry fields or in literatures, the synthesis process inevitably needs the separation of these catalysts from the polyol esters mixture [30,31]. Compared with the above catalysts, Zr-ZSM-5-st not only improved catalytic mass transfer ability, but also produced less metal ion residue. Therefore, it has a good catalytic effect on the oil synthesis reaction.

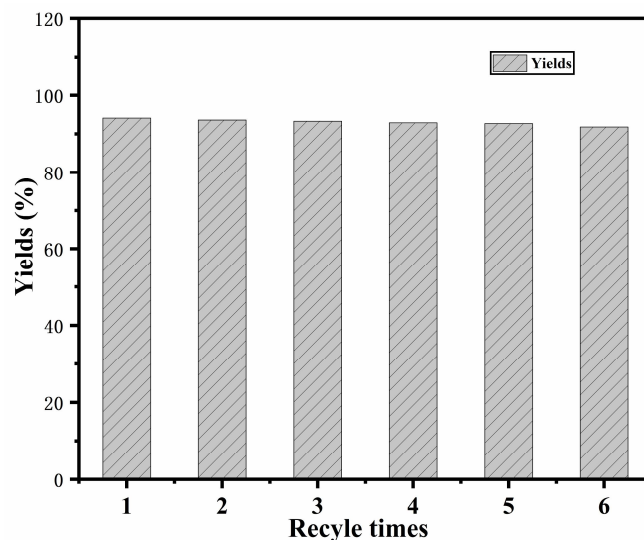


Figure 5. The reusability of Zr(40)-ZSM-5-st(500) for esterification.

3. Materials and Methods

3.1. Catalyst Preparation

ZSM-5 synthesis: In this study, ZSM-5 catalyst (Al/Si ratio, 1:30) was prepared as follows. First, 33.4 mL tetraethylorthosilicate (TEOS, 99.99 wt%, Aladdin, Shanghai, China) was mixed with 34.5 mL tetrapropylammonium hydroxide solution (TPAOH, 25.0 wt%, Cairui, Shanghai, China) under stirring at 40 °C for 1 h. Next, 0.76 g aluminum isopropoxide (AIP, 99.99%, Aladdin, Shanghai, China) was hydrolyzed in 75 mL deionized (DI) water (Prepared in laboratory) for a 1.5 h-period at 85 °C. Subsequently, under the stirring condition, the aluminum-containing solution was subsequently dropped into the silicone-containing solution. Next, we added the resultant solution into the Teflon-lined stainless steel autoclave (Changyi, Xi'an, China) to heat for a 72 h-period at 170 °C. After cooling to ambient temperature post-crystallization, products were subject to centrifugation, washing, and drying overnight. Finally, the template was eliminated through calcination at 550 °C for obtaining the ZSM-5 catalyst.

Post-treatment of ZSM-5: The ZSM-5 catalyst was treated with steam within the horizontal quartz tube oven (Kejing, Hefei, China). Next, 0.5 g ZSM-5 powder was heated until the desired temperature (400–700 °C) at the 10 °C/min rate. Subsequently, to introduce steam, the N_2 steam (100 mL/min) was passed through a water-containing saturator at 80 °C (water partial pressure, 47.4 KPa). We maintained the steam flow at 90 mL/min. These zeolite samples were named ZSM-5-st(x), in which x represents the steaming temperature (400, 500, 600 and 700 °C). The ZSM-5-st samples were post-treated in an H_2ZrF_6 solution at room temperature as follows: a certain amount of H_2ZrF_6 (45.0 wt.% in H_2O) and ZSM-5-st powder were dissolved into DI water for 1 h with stirring. The molar composition of the synthetic solution was 1.0 $SiO_2:mH_2ZrF_6:83.3 H_2O$. The products were centrifuged, washed, and dried at 200 °C to obtain the final Zr(y)-ZSM-5-st catalyst, where y represents the Si/Zr molar ratio (12, 40, 67, 133).

3.2. Catalyst Characterization

The Rigaku D/Max2550VB/PC X-ray diffractometer (Rigaku, Tokyo, Japan) was utilized to collect the X-ray diffraction patterns (XRD) with Cu-K α radiation. The Nicolet NEXUS 670 spectrometer (Nicolet, Madison, KY, USA) was used to obtain Fourier transform infrared spectroscopy (FT-IR) spectra by using KBr as the background. The Perkin-Elmer Lambda 35 spectrophotometer (Perkin-Elmer, Waltham, WA, USA) was used for determining ultraviolet-visible spectroscopy (UV-vis) spectra within the range 200–800 nm, with pure BaSO₄ as the control. The Micromeritics ASAP 2020 machine (Micromeritics, Norcross, GA, USA) was used for measuring N₂ adsorption-desorption isotherms. Furthermore, the JEOL JSM-2100 microscope (JEOL, Tokyo, Japan) was used for obtaining TEM images. Next, Quantachrome ChemBET TPR/TPD (Anton Paar QuantaTec, Boynton Beach, FL, USA) was applied for obtaining ammonia temperature-programmed desorption (NH₃-TPD) spectra. The Perkin-Elmer PHI 5000C ESCA system (Perkin-Elmer, Waltham, WA, USA) was used for performing XPS spectra. Zr and Al contents of Zr-ZSM-5-st catalysts were measured using the Agilent 730 ICP-OES spectrometer (Agilent, Santa Clara, CA, USA).

3.3. Activity Test

The conditions for esterification reaction were described as follows. First, trimethylolpropane (Macklin, Shanghai, China) was esterified with *n*-caprylic acid (Macklin) within the 100 mL three-necked round-bottomed flask (Shuniu, Chengdu, China) under magnetic stirring. Subsequently, we added catalyst (0.5 wt%), 0.015 mol trimethylolpropane (2.01 g), as well as 0.045 mol *n*-caprylic acid (trimethylolpropane to *n*-caprylic acid ratio, 1:3). Additionally, 3 mL toluene (Sinopharm chemical reagent co., Ltd, Shanghai, China) was added to be the water-removing agent for a 5 h-reaction under 160 °C. Next, the mixed solution was centrifuged for collecting the Zr-ZSM-5-st catalyst, which was then subjected to vacuum drying before subsequent use. The solution was concentrated under rotational evaporation for producing ester, and those by-products (water, nonreacted substrates) were eliminated.

To test the reusability of the chosen Zr(12)-ZSM-5-st(500) catalyst, the aforementioned process was repeatedly conducted with the catalyst used. In addition, HR-MS and ¹H NMR were conducted for identifying products, with triphenylmethane used as the endogenous reference to determine the yield based on ¹H NMR. Supplementary materials display details of the procedure.

4. Conclusions

Zr active species were implanted into the ZSM-5 zeolite framework to form a solid acid catalyst through steam treatment and liquid–solid isomorphous substitution process. The synthesis conditions of the Zr-ZSM-5-st catalysts were systematically investigated, and the optimum synthesis conditions were determined. The as-synthesized Zr(40)-ZSM-5-st(500) catalyst revealed superb catalytic activity in the esterification of trimethylolpropane and FAs, with polyol esters production reaching 94.41%. FT-IR, XRD, N₂ physisorption, UV-vis, TEM-mapping, XPS, NH₃-TPD and ICP, the structure-performance relationship of the catalyst was clarified. The excellent catalytic performance of Zr-ZSM-5-st can be attributed to the following causes. First, the implanted framework Zr species increases the acidity of the catalyst, which provides catalytic active sites; second, the developed surface area and pore structure of Zr-ZSM-5-st is conducive to the improvement of catalytic mass transfer ability.

Supplementary Materials: The following supporting information can be downloaded at: <https://www.mdpi.com/article/10.3390/catal12080901/s1>, Figure S1: XRD patterns of Zr(40)-ZSM-5-st treated at 400–700 °C (a) and Zr-ZSM-5-st(500) with Si/Zr mole ratio of 12–133 (b); Figure S2: TEM images of ZSM-5 zeolite; Figure S3: NH₃-TPD spectra of Zr(40)-ZSM-5-st treated at 400–700 °C (a) and Zr-ZSM-5-st(500) with Si/Zr mole ratio of 12–133 (b); Table S1: Surface area and pore volume distribution of ZSM-5, Zr-ZSM-5 and a series of Zr-ZSM-5-st catalysts.

Author Contributions: Conceptualization, H.S. and Z.S.; methodology, H.S., Z.Z., X.F., X.W. and Y.Q.; software, H.S., Z.S.; validation, H.S., W.L., Z.S. and X.F.; formal analysis, H.S., Q.Z. and Z.S.; investigation, H.S., W.L., X.W., Y.Q. and X.F.; resources, W.L. and Y.Q.; data curation, H.S., Z.Z. and Z.S.; writing—original draft preparation, H.S.; writing—review and editing, H.S., Z.S., Q.Z., Y.Q. and W.L.; visualization, H.S. and Z.S.; supervision, Z.S. and Y.Q.; project administration, Z.S.; funding acquisition, W.L., X.F. All authors have read and agreed to the published version of the manuscript.

Funding: This work was supported by the National Natural Science Foundation of China NSFC (NSFC 51775536) and the Natural Science Foundation of China (No. 21978325, 21776312).

Institutional Review Board Statement: Not applicable.

Informed Consent Statement: Not applicable.

Data Availability Statement: For more detailed data, please request from the corresponding authors.

Conflicts of Interest: The authors declare no conflict of interest.

References

1. Su, H.G.; Zhao, Q.; Wang, Y.N.; Zhao, Q.L.; Jang, C.; Niu, Y.F.; Lou, W.J.; Qi, Y.X. SnO nanoparticles on graphene oxide as an effective catalyst for synthesis of lubricating ester oils. *Catal. Commun.* **2022**, *162*, 106370–106374. [[CrossRef](#)]
2. Wang, Y.N.; Ma, R.; Jiang, C.; Lou, W.; Wang, X.B. An efficient catalyst COK-15b for the catalytic synthesis of lubricating ester oils. *Catal. Commun.* **2019**, *122*, 28–32. [[CrossRef](#)]
3. Yu, S.T.; Wu, S.S.; Li, L.; Ge, X.P. Upgrading bio-oil from waste cooking oil by esterification using $\text{SO}_4^{2-}/\text{ZrO}_2$ as catalyst. *Fuel* **2020**, *276*, 118019–118024. [[CrossRef](#)]
4. Yu, G.X.; Zhou, X.L.; Li, C.L.; Chen, L.F.; Wang, J.A. Esterification over rare earth oxide and alumina promoted $\text{SO}_4^{2-}/\text{ZrO}_2$. *Catal. Today* **2009**, *148*, 169–173. [[CrossRef](#)]
5. Zaccheria, F.; Mariani, M.; Psaro, R.; Bondioli, P.; Ravasio, N. Environmentally friendly lubricants through a zero waste process. *Appl. Catal. B-Environ.* **2016**, *181*, 581–586. [[CrossRef](#)]
6. Choi, M.; Na, K.; Kim, J.; Sakamoto, Y.; Terasaki, O.; Ryoo, R. Stable single-unit-cell nanosheets of zeolite MFI as active and long-lived catalysts. *Nature* **2009**, *461*, 246–249. [[CrossRef](#)]
7. Forde, M.M.; Armstrong, R.D.; Hammond, C.; He, Q.; Jenkins, R.L.; Kondrat, S.A.; Dimitratos, N.; Lopez-Sanchez, J.A.; Taylor, S.H.; Willock, D.; et al. Partial oxidation of ethane to oxygenates using Fe- and Cu- containing ZSM-5. *J. Am. Chem. Soc.* **2013**, *135*, 11087–11099. [[CrossRef](#)]
8. Shang, J.Y.; Fu, G.B.; Cai, Z.P.; Feng, X.; Tuo, Y.X.; Zhou, X.; Yan, H.; Peng, C.; Jin, X.; Liu, Y.B.; et al. Regulating light olefins or aromatics production in ex-situ catalytic pyrolysis of biomass by engineering the structure of tin modified ZSM-5 catalyst. *Bioresour. Technol.* **2021**, *330*, 124975. [[CrossRef](#)] [[PubMed](#)]
9. Tu, C.Y.; Fan, H.H.; Wang, D.; Rui, N.; Du, Y.H.; Senanayake, S.D.; Xie, Z.H.; Nie, X.W.; Chen, J.G. CO_2 -assisted ethane aromatization over zinc and phosphorous modified ZSM-5 catalysts. *Appl. Catal. B-Environ.* **2022**, *304*, 120956. [[CrossRef](#)]
10. Wang, H.R.; Li, X.C.; Meng, F.R.; Wang, G.Y.; Zhang, D.K. Preparation and evaluation of iron nanoparticles embedded CNTs grown on ZSM-5 as catalysts for NO decomposition. *Chem. Eng. J.* **2020**, *392*, 123798. [[CrossRef](#)]
11. Mohebbi, S.; Rostamizadeh, M.; Kahforoushan, D. Efficient sulfated high silica ZSM-5 nanocatalyst for esterification of oleic acid with methanol. *Micropor. Mesopor. Mat.* **2020**, *294*, 109845. [[CrossRef](#)]
12. Mahyuddin, M.H.; Staykov, A.; Shiota, Y.; Yoshizawa, K. Direct conversion of methane to methanol by metal-exchanged ZSM-5 zeolite (metal = Fe, Co, Ni, and Cu). *ACS Catal.* **2016**, *6*, 8321–8331. [[CrossRef](#)]
13. Hou, X.; Qiu, Y.; Tian, Y.J.; Diao, Z.H.; Zhang, X.W.; Liu, G.Z. Reaction pathways of *n*-pentane cracking on the fresh and regenerated Sr, Zr and La-loaded ZSM-5 zeolites. *Chem. Eng. J.* **2018**, *349*, 297–308. [[CrossRef](#)]
14. Fan, M.J.; Si, Z.K.; Sun, W.J.; Zhang, P.B. Sulfonated $\text{ZrO}_2\text{-TiO}_2$ nanorods as efficient solid acid catalysts for heterogeneous esterification of palmitic acid. *Fuel* **2019**, *252*, 254–261. [[CrossRef](#)]
15. Popova, M.; Lazarova, H.; Kalvachev, Y.; Todorova, T.; Szegedi, Á.; Shestakova, P.; Mali, G.; Dasireddy, V.D.B.C.; Likozar, B. Zr-modified hierarchical mordenite as heterogeneous catalyst for glycerol esterification. *Catal. Commun.* **2017**, *100*, 10–14. [[CrossRef](#)]
16. Li, G.; Gao, L.; Sheng, Z.Z.; Zhan, Y.L.; Zhang, C.Y.; Ju, J.; Zhang, Y.H.; Tang, Y. A Zr-Al-Beta zeolite with open Zr(IV) sites: An efficient bifunctional Lewis-Brønsted acid catalyst for a cascade reaction. *Catal. Sci. Technol.* **2019**, *9*, 4055–4065. [[CrossRef](#)]
17. Groen, J.C.; Moulijn, J.A.; Pérez-Ramírez, J. Decoupling mesoporosity formation and acidity modification in ZSM-5 zeolites by sequential desilication-dealumination. *Micropor. Mesopor. Mat.* **2005**, *87*, 153–161. [[CrossRef](#)]
18. Yang, Y.; Zhou, D.; Zhang, H.X.; Yin, B.Y.; Liu, Q.R.; Lu, X.H.; Yang, S.J.; Xia, Q.H. In-situ construction and catalytic property of highly exposed Lewis acidity on hierarchical Zr-zeolite assisted by K^+ cation. *Micropor. Mesopor. Mat.* **2021**, *324*, 110898. [[CrossRef](#)]
19. Li, X.C.; Yuan, X.H.; Xia, G.P.; Liang, J.; Liu, C.; Wang, Z.D.; Yang, W.M. Catalytic production of γ -valerolactone from xylose over delaminated Zr-Al-SCM-1 zeolite via a cascade process. *J. Catal.* **2020**, *392*, 175–185. [[CrossRef](#)]

20. Miyake, N.; Brezicki, G.; Davis, R.J. Cascade reaction of ethanol to butadiene over multifunctional silica-supported Ag and ZrO₂ Catalysts. *ACS Sustain. Chem. Eng.* **2022**, *10*, 1020–1035. [[CrossRef](#)]
21. Liao, Y.H.; Zhong, R.Y.; d'Halluin, M.; Verboekend, D.; Sels, B.F. Aromatics production from lignocellulosic biomass: Shape selective dealkylation of lignin-derived phenolics over hierarchical ZSM-5. *ACS Sustain. Chem. Eng.* **2020**, *8*, 8713–8722. [[CrossRef](#)]
22. Holzinger, J.; Beato, P.; Lundegaard, L.F.; Skibsted, J. Distribution of aluminum over the tetrahedral sites in ZSM-5 zeolites and their evolution after steam treatment. *J. Phys. Chem. C* **2018**, *122*, 15595–15613. [[CrossRef](#)]
23. Xue, Y.F.; Niu, Y.L.; Zheng, H.Y.; Cui, X.J.; Ma, Q.G.; Tang, J.K.; Deng, L.F. Selective dealumination of ZSM-5 by steaming and its effect on ethanol to propene. *J. Fuel Chem. Technol.* **2021**, *49*, 1111–1121. [[CrossRef](#)]
24. Yang, B.T.; Jiang, J.G.; Zhang, K.; Wu, P. Synthesis of novel titanosilicate catalysts by simultaneous isomorphous substitution and interlayer expansion of zeolitic layered silicates. *Chem. Mater.* **2016**, *28*, 5295–5303. [[CrossRef](#)]
25. Miyake, K.; Inoue, R.; Miura, T.; Nakai, M.; Al-Jabri, H.; Hirota, Y.; Uchida, Y.; Tanaka, S.; Miyamoto, M.; Inagaki, S.; et al. Improving hydrothermal stability of acid sites in MFI type aluminosilicate zeolite (ZSM-5) by coating MFI type all silica zeolite (silicalite-1) shell layer. *Micropor. Mesopor. Mat.* **2019**, *288*, 109523. [[CrossRef](#)]
26. Kis, A.K.; Omota, F.; Dimian, A.C.; Rothenberg, G. The heterogeneous advantage: Biodiesel by catalytic reactive distillation. *Top. Catal.* **2006**, *40*, 141–150. [[CrossRef](#)]
27. Breck, D.W. *Zeolite Molecular Sieves, Structure, Chemistry and Use*; John Wiley & Sons: New York, NY, USA, 1974.
28. Sani, Y.M.; Alaba, P.A.; Raji-Yahya, A.O.; Aziz, A.R.A.; Daud, W.M.A.W. Facile synthesis of sulfated mesoporous Zr/ZSM-5 with improved Brønsted acidity and superior activity over SZr/Ag, SZr/Ti, and SZr/W in transforming UFO into biodiesel. *J. Taiwan Ins. Chem. E.* **2016**, *60*, 247–257. [[CrossRef](#)]
29. Almutairi, S.M.T.; Mezari, B.; Pidko, E.A.; Magusin, P.C.M.M.; Hensen, E.J.M. Influence of steaming on the acidity and the methanol conversion reaction of HZSM-5 zeolite. *J. Cata.* **2013**, *307*, 194–203. [[CrossRef](#)]
30. Kuzminska, M.; Backov, R.; Gaigneaux, E.M. Behavior of cation-exchange resins employed as heterogeneous catalysts for esterification of oleic acid with tri-methylolpropane. *Appl. Catal. A: Gen.* **2015**, *504*, 11–16. [[CrossRef](#)]
31. Åkerman, C.O.; Hagström, A.E.V.; Mollaahmad, M.A.; Stefan, K.B.; Hatti-Kaul, R. Bio-lubricant synthesis using immobilised lipase: Process optimization of tri-methylolpropane oleate production. *Process Bio. Chem.* **2011**, *46*, 2225–2231. [[CrossRef](#)]